Progress In Electromagnetics Research C, Vol. 125, 161–177, 2022

Printed Fractal Folded Coplanar-Strips-Fed Array Rectenna for IoE Applications

Zahra Badamchi[1, *], Ngoc Duc Trinh[2], Chloe Bois[2], and Tarek Djerafi[1]

Abstract—This paper presents a low-cost antenna integrable to a large set of indoor common building materials. Employing the printing technology on thin transparent polyethylene terephthalate material and using available building materials not only leads to a low-cost environmentally friendly solution for the expected massive sensor deployment but also eliminates the dispersive behavior of the materials that are interacting with them. A coplanar-strips fed fractal folded antenna element was designed and validated experimentally with four different materials including gypsum, plywood, and plexiglass. The aesthetically viable ground-free antenna achieves wideband performance and radiates in the broadside plane perpendicularly to the wall. The single antenna element covers the frequency band of 2.18–3.96 GHz with a gain of 1 dBi at 2.4 GHz. To take advantage of the large available surface, a high efficiency 2.4 GHz array rectenna for powering electronic devices intended for IoE technology is proposed. The proposed array rectenna has a dimension of $384 \times 354 \times 6.475\,\text{mm}^3$ and employs a single diode as the rectifier element. The measured results for the presented array rectenna reveal an AC-DC power-conversion-efficiency (PCE) of more than 20% for input powers as low as $0.025\,\mu\text{W/cm}^2$ with a peak PCE of 61.3% at $4.03\,\mu\text{W/cm}^2$.

1. INTRODUCTION

The emergence of the internet of everything (IoE) as an evolution of the internet of things (IoT) promises the concept of smart management of the environment at homes, factories, and cities. The IoE provides the connection of people, sensors, and machines to the Internet, and so they can be considered as parts of the information network [1–5]. The implementation of the IoE requires extensive installation of sensors in the buildings to detect variations of the environment in terms of moisture, temperature, etc. [1–3]. Due to their number and proximity, the sensors should be small, affordable, and energy-efficient [5]. Due to the advancements in low-power consuming semiconductor technologies, batteries can be used to power the IoE sensors; however, replacing or replenishing of such huge number of batteries will not only be time-consuming and laborious, but also produce a huge disposal. Moreover, in many instances the sensors may be installed at a unreachable location, for example inside the building's ceilings or walls, which makes their maintenance harder. Harvesting the unused renewable energy sources in nature and human environments such as mechanical, acoustic, electromagnetic, and thermal energies is one of the most promising solutions for massive deployment of the IoE technology [6, 7]. Among these solutions, the wireless electromagnetic power transfer and harvesting has attracted tremendous attention, recently. Rectennas capable of converting the radio frequency (RF) energy to direct current (DC) energy are the main role-playing device in any RF wireless power transfer system. Therefore, recently several designs of rectennas have been proposed in the literature [8–11].

Received 6 August 2022, Accepted 23 September 2022, Scheduled 16 October 2022
* Corresponding author: Zahra Badamchi (zahra.badamchi@emt.inrs.ca).
[1] Institut National de la Recherche Scientifique-Energie, (INRS), Montréal, QC, Canada. [2] Printability and Graphic Communications Institute (ICI), Montréal, QC, Canada.

In the case of harvesting and wireless transmission of the electromagnetic energy, the larger and more visible part of the sensors is the antenna. The integration of those sensors goes through the integration of the antennas which is more visible part into the environment. The expected massive deployment also adds a strict constraint on the cost and aesthetics issues as well.

In the indoor environment, as illustrated in Fig. 1, the building materials constitute large available surfaces. Other than the metallic one, wood, drywall, and glass are abundant engineering materials with lower costs than the commercial substrates. The integration of the antenna/sensor to those materials will be an asset for the IoE deployment. In [7], a hybrid frequency selective surface (FSS) based rectenna is proposed which can be embedded inside the building's wall to harvest the 2.4 GHz (WLAN) band coverage while being transparent at the 900 MHz cellular band to allow cellphones coverage. However, designing and implementing the antenna/rectennas directly on the existing materials in the building as the main substrate for the antenna and rectifier circuit not only allows large-scale and low-cost implementation of the IoE sensors but also eliminates part of the undesired effect of the environment on the performance of the wireless communication system as well for radiofrequency energy harvesting (RFEH) applications. The signal distortion, caused by the dispersion of the complex permittivity, deteriorates the performance of the rectennas. This is more critical for devices that are printed on a thin substrate and do not have a ground plane on the other side. After installation on the wall, the performance of the antenna is mostly dominated by the complex permittivity of the wall material which affects the frequency response severely [12–17].

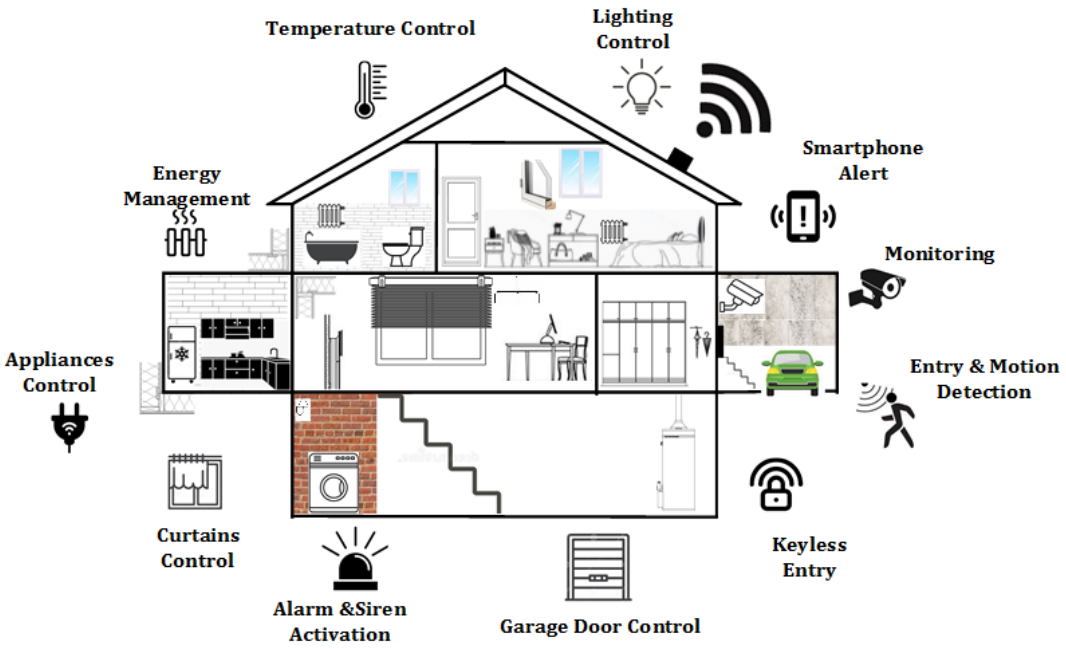

Figure 1. Smart building concept.

In this paper, a printed fractal coplanar-strips-fed array rectenna is presented. The proposed antenna uses a stacked polyethylene terephthalate (PET) sheet and drywall (composed of gypsum material) as the substrate material. Since the drywall is the most commonly available material in any building structure, this merit enables the proposed antenna to be directly employed at any position of the indoor space, while eliminating the concerns about the installation problems which are mostly due to the dispersive behavior of the materials. The performance of the antenna element integrated into the different building materials has been studied. As an application example, a rectenna consisting of a flexible transparent array antenna and rectifying circuit printed with the same process and integrated on gypsum drywall is implemented. The simulated and measured results demonstrate that the proposed rectenna can be a potential candidate for powering indoor distributed sensors and IoE devices.

2. ANTENNA DESIGN, FABRICATION AND EXPERIMENTAL VALIDATION

Among the antennas built on a substrate other than the common commercial dielectrics, the textile-based ones have received the greatest attention [18]. Some researchers use the wood-based as well as bio-composite substrates to create new green technology compatible printed circuit board (PCB) components and antennas [19]. In [20], ultra-high-frequency (UHF) radio frequency identification (RFID) tag antennas manufactured by brush-painting directly on a wood veneer substrate were examined. Some designs also proposed the use of plexiglass and glass as well to take advantage of their transparency [21, 22].

In this section, a fractal folded antenna element design is studied to cover a set of indoor engineering materials but principally the gypsum drywall. A printing technique compatible with mass production is used to estimate the possibility to cover large surfaces in the future with a low-cost process. The design procedure, experimental validation, and fabrication constraints will be detailed in the next subsections.

2.1. Common Dielectric Materials Used in Buildings

The wide variety of building materials makes it very difficult to accurately predict attenuation without the support of specific building data or measurements. The drywalls are large and rigid sheets that are fastened directly to the frame of the building with nails, screws, or adhesives, and are mounted on furring. The common materials used in drywall are gypsum boards, plywood, fiber-and-pulp boards, and asbestos-cement boards.

A review of the dielectric and magnetic properties measurements method for lossy materials including building materials is presented in [13]. The dielectric properties of typical building materials have been estimated from transmission and reflection measurements at 41.5 GHz and 5.8 GHz bands in [14], and at 5.8 GHz and 62.4 GHz in [15]. The permittivity measurement of concrete consisting of aggregates of up to 30 mm in the frequency range of 50 MHz–1 GHz is estimated with a new dielectric measurement method in [16], and a new planar microwave sensor composed of a log-periodic antenna was developed to characterize the relative permittivity of concrete blocks in [17]. An extensive ultra-wideband measurement of the complex permittivity for the common building materials has been performed in [12]. Table 1 lists some of the obtained results at 2.4 GHz. According to these results, gypsum material has a dielectric constant of $\varepsilon_{r\text{gypsum}} = 2.7$ and a dielectric loss tangent of $\tan\delta_{\text{gypsum}} = 0.05$. The relatively low loss performance of the gypsum enables it to be used directly as the substrate.

Table 1. Common dielectric materials used in buildings, (Values are for 2.4 GHz).

Substrate	Dielectric constant (ε_r)	Dielectric loss (tan)	Thickness (mm)
Gypsumplaster (drywall)	2.7	0.01	6.35
Glass	6.4	0.01	5
Plexiglass	3.2	0.001	5.5
Red brick	3.2	0.01	6.5
Concrete	4	0.02	6
Plywood	2.5	0.11	6

In the current research, in order to obtain the electromagnetic characteristic parameters of the utilized drywall under realistic building conditions including room temperature and humidity, practical measurements were performed in the lab. Coaxial probe method was performed using Keysight 85070B high temperature dielectric probe kit, Keysight N5247B PNA-X, and Keysight N1500A materials measurement suite software. The under-test drywall sample has a thickness of 6.35 mm. Several measurements were performed at multiple random points on the substrate and then averaged to increase the measurement accuracy. The obtained results for the dielectric constant over the frequency are

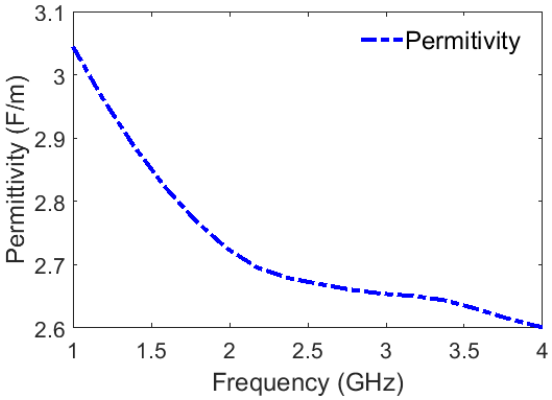

Figure 2. Measured dielectric constant of the gypsum sample.

depicted in Fig. 2. According to these results, the corresponding dielectric constant of the drywall is $\varepsilon_r = 2.66$ at 2.4 GHz. This value was used during the simulation studies to ensure their validity.

2.2. Printing Technique and Materials

Printed electronics can be employed to develop RF circuits on almost any material such as textiles, paper, wood, glass, metal, ceramic, and plastic. This method is more environmentally friendly in comparison with the methods which require chemical etching such as conventional PCB technology. Moreover, the printed circuits possess the potential to provide biodegradable and recyclable solutions to minimize the electronic waste caused by the increasing number of disposed electronic devices. For this work, the screen-printing technique is used. The screen-printing technique is a simple and low-cost method that is suitable for large-size antennas and massive industrial production. Its operation is quite straightforward. A flood blade moves along the screen and fills the open mesh areas with the conductive ink. Then by moving a squeegee in the reverse direction of the flood blade, the trapped ink in the mesh aperture is transferred to the substrate surface which is placed beneath it. Fig. 3 shows the EKRA X1-SL Semi-Automatic Screen Printer which has a repetition accuracy of 15 µm depending on screens selection. The employed screen has a mesh count of 92 fibers/cm.

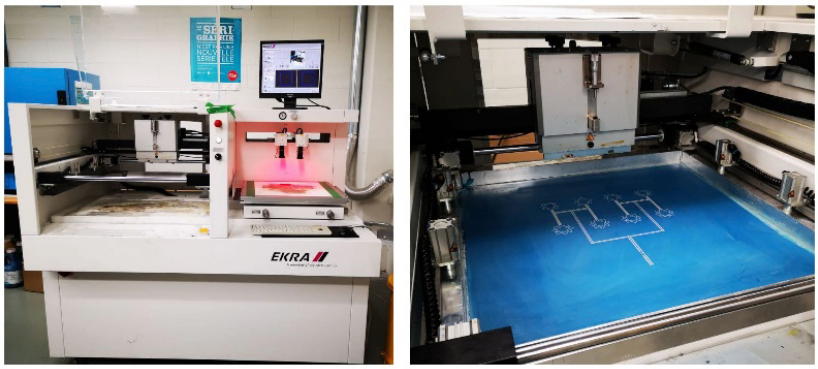

Figure 3. Semi-automatic screen printer EKRA X1 SL.

A thin PET sheet with a thickness of $h_{\mathrm{PET}} = 125\,\mu\mathrm{m}$, a dielectric constant of $\varepsilon_{r\mathrm{PET}} = 3$, and a dielectric loss tangent of $\tan\delta_{\mathrm{PET}} = 0.001$ is placed under the screen as the primary substrate on which the conductive sections are printed [23]. The thickness of the used PET is negligible in comparison to the drywall material. Transparency is desirable as it facilitates the attachment to different substrates. Transparency enables large-scale array rectennas to integrate better into urban environments while preventing the shadowing of the sun.

The HPS-021LV water-based silver flake ink from Novacentrix company [24] with a conductivity of $\sigma = 8 \times 10^4\,\Omega/\mathrm{m}$, calculated from previous tests using flat-bed screen printing, is selected for this work, as it allows low-cost massive implementation of the IoE technology. After printing, the sintering process is necessary to ensure suitable conductivity of the printed sections. The curing temperature depends on the temperature tolerance of the substrate. Lower curing temperature leads to the remaining large gaps between the ink particles. Increasing the temperature ensures the removal of residual solvent and the conductive particles pack together and gaps start to vanish, which provides a continuous smoothness of the conductor, and thereby an efficient percolation channel is created for the electrons to flow along. The employed PET substrate for this work has a heat shrinkage of less than 1%, and the print is cured in the oven for 20 minutes at 90°C.

The surface resistance (R_s) per unit length of the printed product is severely affected by the roughness of the conductive section. This can be described by [25]:

$$\begin{aligned} R_s &= cR, \\ c &= \left(1 + \frac{2}{\pi}\tan^{-1}\left(1.4 \times \left(\frac{S_a}{\delta}\right)\right)\right), \\ R &= \frac{1}{\omega}\sqrt{\frac{\pi\mu f}{\sigma}} \\ \delta &= \sqrt{\frac{R}{\pi f \mu_r \mu_0}} \end{aligned} \tag{1}$$

where c is the correction factor; R is the initial value for surface resistivity; f is the frequency; $\mu_r \approx 1$ is the relative permeability of the conductor; $\mu = 4 \times \pi \times 10^{-7}$ is the vacuum permeability; S_a is mean surface roughness; σ is the conductivity of the ink; and δ is the skin-depth. The resistive loss increases drastically when the surface roughness is comparable to the skin depth of the electromagnetic wave at

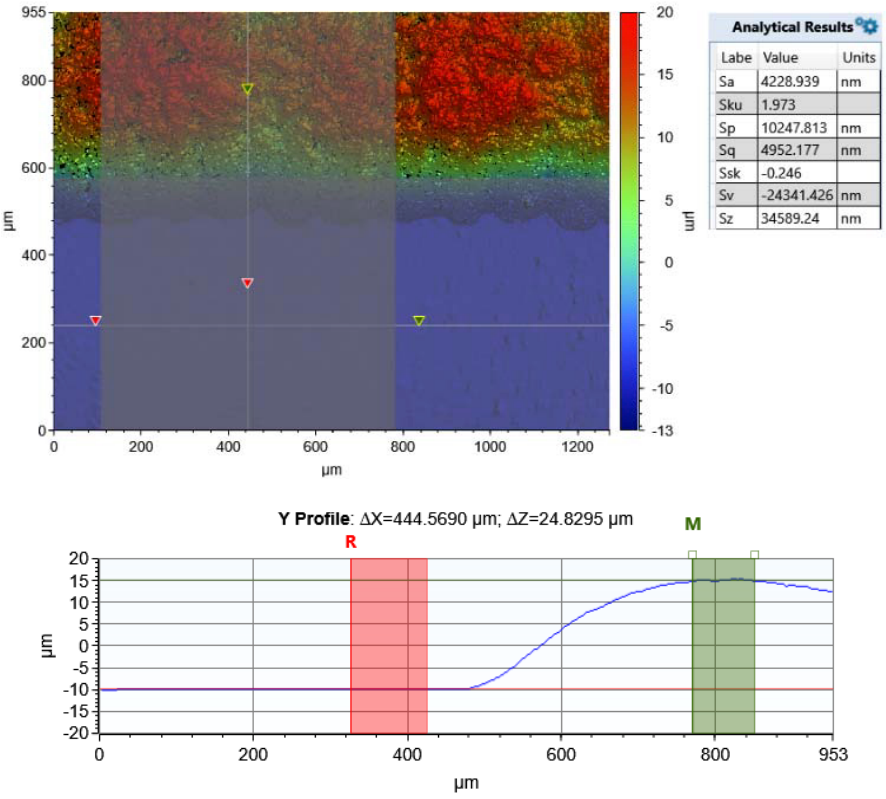

Figure 4. Colored optical image of 2D surface roughness graph and extracted data.

the operating frequency. In this work, the roughness of the cured silver pattern is determined by taking its height profile using the Bruker Contour GT-K 3D optical microscope [26]. The optical image with the extracted results for the roughness is depicted in Fig. 4. The cured print possesses a mean surface roughness of $S_a = 4.22\,\mu\text{m}$.

The resulting dried silver film thickness was measured using TMI Digital Micrometer Model 49-86 [27], and is $t = 24 \pm 2\,\mu\text{m}$ over the realized prototype. The sheet resistance of the printed product was measured using the Signatone four-point probe [28], and is $R_s = 0.052\,\text{ohm/sq}$. The relation between the sheet resistance of the printed conductive ink and its thickness can be expressed as:

$$R_s = \frac{R}{t} \tag{2}$$

Thereby, dried silver film track skin depth is calculated to be $\delta = 11.49\,\mu\text{m}$ at $2.4\,\text{GHz}$. Satisfying $S_a < \delta < t$ guarantees low loss performance of the printed prototype.

In order to attach the lumped element components of the rectenna to the printed structure, Sun Chemical AST6320 silver ink is used which is supplied as ready-to-use ink. It can be applied at the room temperature. Drying time may range from 1–30 minutes.

2.3. Single Antenna Element

The proposed single antenna element is composed of a fractal-shaped folded radiating element that is connected to a coplanar-strips (CPS) feedline for signal transmission as shown in Fig. 5. This type of line allows the design of a structure without ground. It aspires to achieve wide bandwidth and cover the usage of different substrate materials. Initially, the printed structure is stacked on a second thicker gypsum substrate with a thickness of $h_{\text{gyp}} = 6.35\,\text{mm}$, and thereby the proposed antenna is formed.

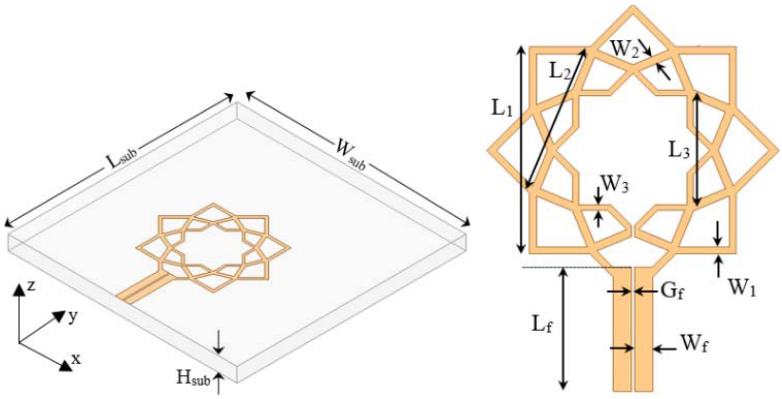

Figure 5. Designed fractal CPS-fed folded antenna: (a) structure, and (b) printed conductive section.

CPS is basically similar to coplanar waveguide (CPW), and is a transmission line that has a structure complementary to that of CPW. Inherently, the CPS is a balanced line type that transmits signals through two lines, and its basic purpose and characteristics are the same as those of the CPW. The main difference from the CPW is the fact that its characteristic impedance is several times larger for a structure with a similar size and requires the use of a lower quantity of conductor material. CPS feeding is adopted to reduce the risk of ink permeation as it requires no ground plane. It is important to mention that the characteristics of the CPS remain constant when the thickness of the substrate is greater than or comparable to the dimensions of the transmission line section [29].

Ansys HFSS software was used to design and simulate the antenna element. The final values for the antenna design parameters are listed in Table 2. The fractal geometry for the radiating section is chosen to increase the frequency bandwidth of operation. Fig. 6 shows various structures which were investigated during simulation studies in terms of matching and gain, and their performances are

Table 2. Design parameters values of the antenna element.

Param	Value (mm)	Param	Value (mm)
L_{sub}	100	L_2	26
W_{sub}	100	L_3	19.9
L_f	20.44	W_1	1.14
W_f	3	W_2	1.46
G_f	0.5	W_3	1
L_1	34	H_{sub}	6.475

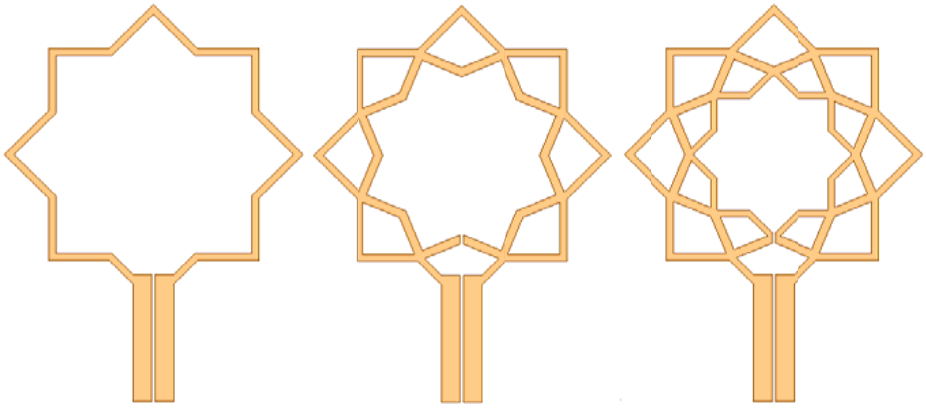

(a) (b) (c)

Figure 6. Various studied fractal steps: (a) single ring fractal folded antenna, (b) dual ring fractal folded antenna, and (c) triple ring fractal folded antenna.

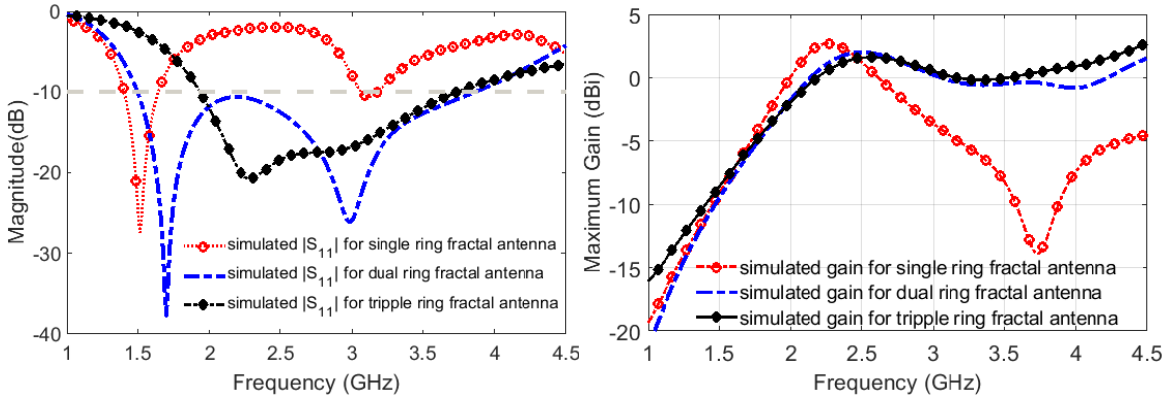

(a) (b)

Figure 7. Simulated results of the antenna element for various fractal steps: (a) reflection coefficient, and (b) gain.

compared in Fig. 7. According to this figure, the covered frequency band increases as the number of the employed fractal rings in the antenna structure increases, and the radiation bandwidth of the proposed antenna covers the frequency band of 2.1–3.8 GHz with a fractional bandwidth of 57%. Moreover, the measured maximum gain results reveal that the proposed antenna element provides a gain level of 1.3 dBi at 2.4 GHz. The simulated results for the proposed antenna structure reveal an input impedance of 120 Ω.

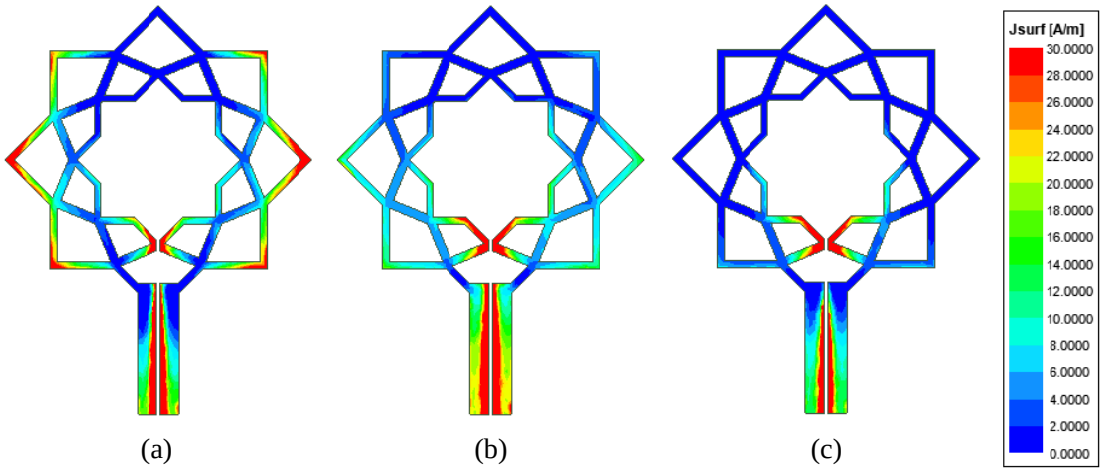

Figure 8. Simulated surface current distribution on the antenna at: (a) 2.4 GHz, (b) 3 GHz, and (c) 3.6 GHz.

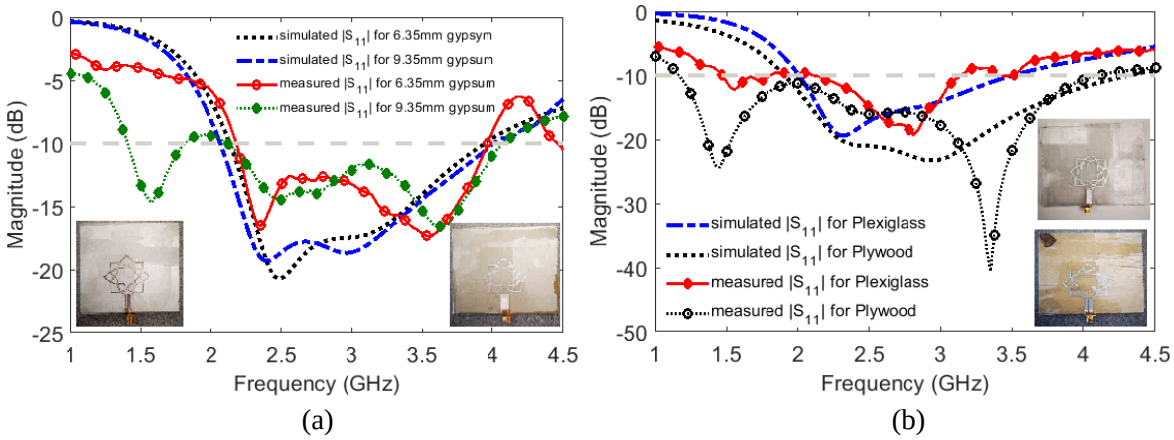

Figure 9. Measured and simulated reflection coefficient of the fabricated antenna elements with fabricated prototypes: (a) gypsum with thickness of 6.35 mm (left side picture), and with thickness of 9.52 mm (right side picture), and (b) plywood with thickness of 6.35 mm (bottom picture), and Plexiglass with thickness of 6.35 mm (top picture).

In order to provide a better insight about the wideband performance of the designed antenna, the surface current distribution on the antenna structure at various frequencies is depicted in Fig. 8. As can be observed in this figure, at lower frequencies the currents are more dominant on the longer paths of the fractal shaped radiator and contribute to the radiation, and as the frequency increases the currents on shorter paths become more dominant and contribute to the radiation. Thereby, a wideband operation is achieved.

Keeping all the designed antenna parameters fixed, the effect of changing the height of the secondary gypsum substrate was investigated. Fig. 9(a) shows the realized antenna elements on gypsum substrates with thicknesses of 6.35 and 9.52 mm, and their simulated and measured reflection coefficient results are compared. According to these results, a fine agreement exists between the simulated and measured results. The antenna realized on the thinner substrate covers the frequency band of 2.18–3.97 GHz, while the antenna realized on the thicker substrate covers the frequency band of 2.14–4.1 GHz.

The performance of the same printed structure when it is stacked on other building materials as the secondary substrate was also investigated. Fig. 9(b) shows the realized antennas on plywood and plexiglass and their simulated and measured reflection coefficient characteristics. According to these

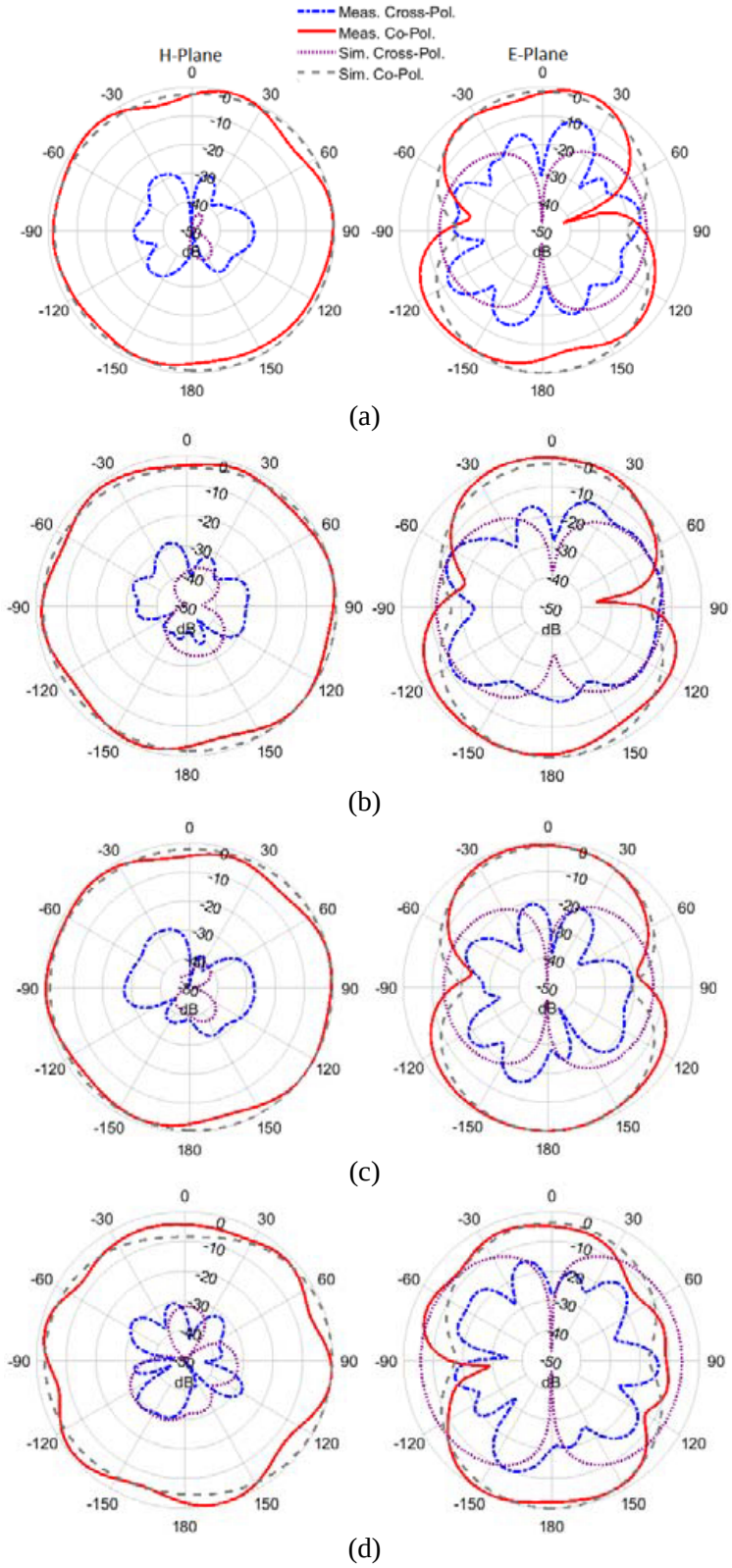

Figure 10. Simulated and measured radiation patterns of the antenna elements: (a) gypsum with 6.35 mm height, (b) gypsum with 9.35 mm height, (c) plywood with 6.35 mm height, and (d) Plexiglass with 6.35 mm height.

results, the fabricated antenna on the plywood covers the frequency band of 1.17–4.13 GHz, while the fabricated antenna on plexiglass covers the frequency band of 2.1–3.15 GHz. A good agreement exists between simulated and measured results, and the resultant antennas can cover ISM band frequencies around 2.4 GHz. This is mainly because according to Table 1 the dielectric constants of plexiglass and plywood materials are close to the dielectric constant of gypsum. So, the same printed structure can be stacked on the various building materials for our intended applications.

The radiation patterns of simulated and measured co-polarization and cross-polarization components for the designed antennas, implemented on various previously mentioned substrates, are plotted in Fig. 10. These results reveal that all of the fabricated antenna elements radiate effectively and have an almost omnidirectional pattern on the H-plane with a very low cross-polarization level. The measured and simulated gain characteristics for the antenna implemented on a 6.35 mm thick gypsum substrate are depicted in Fig. 11. This antenna possesses a gain of 1 dBi at 2.4 GHz.

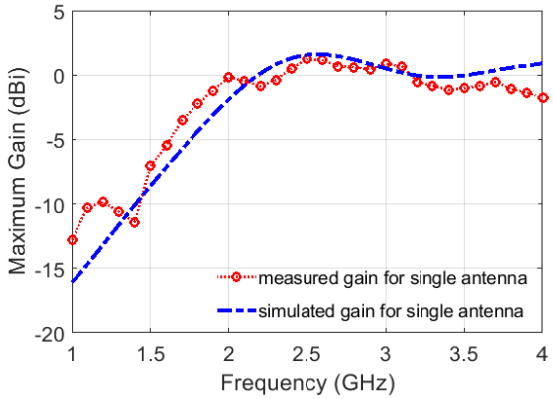

Figure 11. Measured and simulated gain at the direction of the maximum radiation for the single antenna element fabricated on gypsum with a thickness of 6.35 mm.

2.4. Array Antenna

In order to arrange an array antenna on a gypsum substrate with a thickness of 6.35 mm and based on the designed fractal antenna element, a CPS line feed network was designed. In the design of the feed network, two major goals were pursued simultaneously. The first goal was to achieve an array antenna with high aperture efficiency, and the second goal was to minimize the feed-network path loss to avoid losing signal strength while passing through the feed-network toward the rectifier circuit. Fig. 12 depicts the structure of the designed array antenna, and the values for its design parameters are listed in Table 3.

In order to have the received signals by all elements in phase, extended paths were used to connect half of the elements to the feed-network ($Y_1 \approx L_f + \lambda/2$). According to Goverdhanam et

Table 3. Design parameters values of the array antenna.

Param	Value (mm)	Param	Value (mm)
X_1	35	X_2	2
X_3	79.7	X_4	2.5
Y_1	58.6	Y_2	2.8
Y_3	157.5	Y_4	2
Y_5	62	G_1	1.1
G_2	1.7	G_3	1
G_4	2	L_F	16

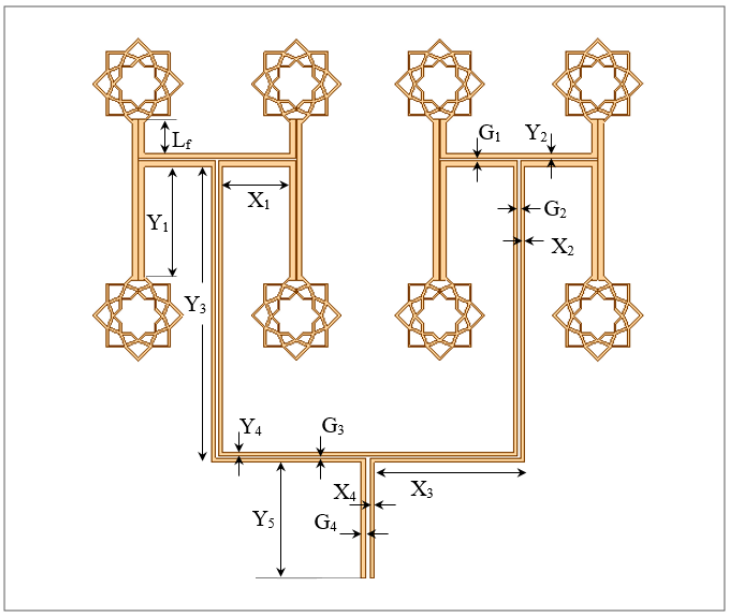

Figure 12. Designed fractal CPS-fed array antenna.

al., compensation of the CPS bend to improve the insertion loss is not required [30]. The number of employed elements was selected by compromising between the insertion loss and achieved gain level. The path loss is mainly affected by the T-junctions. As illustrated in Fig. 12, the feed-network is composed of multiple symmetrically located T-junctions that distribute the signal evenly between the antenna elements. The elements are aligned at a distance of 0.75λ from each other (center to center).

According to simulation results having three sets of symmetrical T-junctions for connecting eight antenna elements imposes 2.1 dB insertion loss to the system. Two prototypes, four elements array, and eight-elements array antennas, without the rectifier section, were fabricated, and their frequency bandwidth characteristics were measured. Fig. 13(a) compares the simulated and measured reflection coefficients for the eight-elements array antenna. According to these results the fabricated eight-elements array antenna is capable of covering the frequency band of 2–2.9 GHz. Same results for the fabricated four-elements array antenna in Fig. 13(b) show that it covers the frequency band of 1.993.43 GHz.

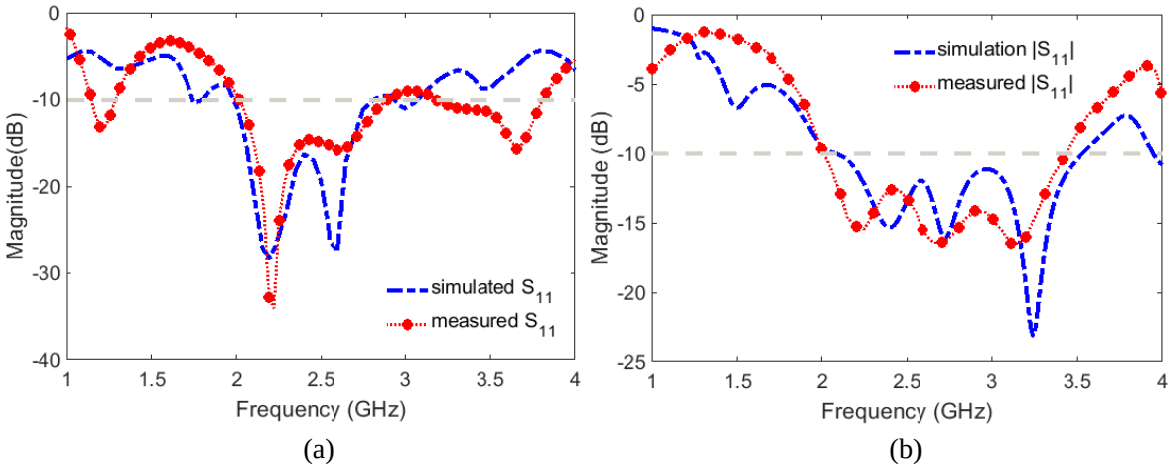

Figure 13. Simulated and measured reflection coefficient of: (a) the eight-elements array antenna, and (b) the four-elements array antenna.

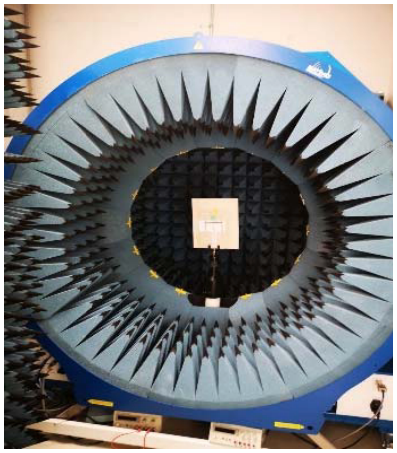

Figure 14. Fabricated four-elements antenna array installed in the anechoic chamber.

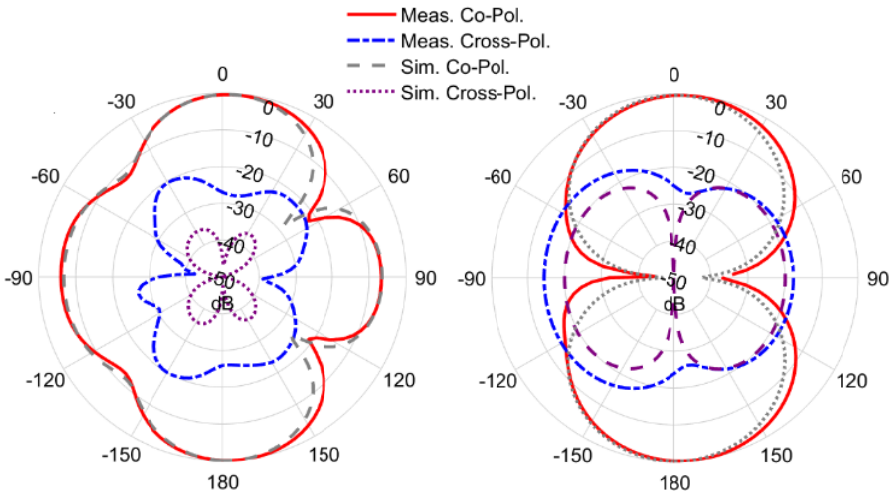

Figure 15. Simulated and measured radiation patterns of the four-elements array antenna.

Due to the restriction on the size of the utilized near-field measurement system, the radiation pattern and gain characteristic of the fabricated eight-elements array could not be measured. Fig. 14 shows the four-elements array placed in an anechoic chamber, and its measured and simulated radiation patterns are compared in Fig. 15. The measured and simulated gain characteristics for this array along with the simulated gain characteristic of the eight-elements array are plotted in Fig. 16. Good agreement exists between the simulated and measured gains for the four-elements array, and the measured gain is 5.5 dBi at 2.4 GHz. Thereby, it can be expected that the fabricated eight-elements array possesses a gain level close to its simulation prediction which is 9.96 dBi at 2.4 GHz. Based on the mentioned results, the number of the employed elements was selected to be eight, and the designed array antenna has an input impedance of 172 Ω.

3. DRY WALL RECTENNA FOR RF POWER HARVESTING

Replacing or replenishing the huge number of batteries associated with the sensors will not only be time-consuming and laborious but also produce huge disposal [4]. Moreover, in several scenarios, the sensors may be installed at a non-reachable location, for example inside the building's ceilings or walls, which makes their maintenance harder. Using rectifying antennas (rectennas) for harvesting the ambient radio-frequency (RF) energy can be a possible solution to overcome this challenge [4, 31]. On the other

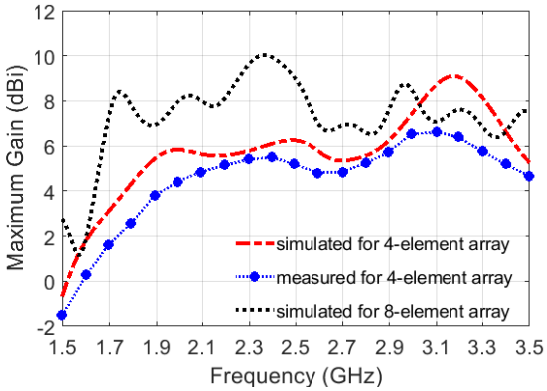

Figure 16. Measured and simulated gain at the direction of the maximum radiation for four-elements antenna array on gypsum with a thickness of 6.35 mm.

hand, several surveys have shown that the major restriction for RFEH systems is the extremely low power density of the ambient RF signals [4]. The proposed technique can be used as an antenna/antenna array associated with sensors as well for power transfer or harvesting of the RF energy. In fact, the use of large surfaces allows the harvesting of more energy. Additionally, for the same power density in space, the high-gain rectennas are more efficient in capturing the energy and delivering it to the rectifier diode than the omnidirectional rectennas with lower gain levels.

The zoomed-in view of the designed rectifier section is depicted in Fig. 17 with the block diagram. The rectifier utilizes a single zero-bias diode (SMS7630 Schottky barrier diode) topology, which is adapted for a low received power application [31]. The spice model of the diode and harmonic balance simulation engine was used in Keysight Advanced Design Software for the design. The diode has a series resistance $R_S = 20\,\Omega$, zero-bias junction capacitance $C_{j0} = 0.14\,\text{pF}$, built-in-turn-on voltage $V_{bi} = 0.34\,\text{V}$, and a breakdown voltage $V_B = 2\,\text{V}$. The balanced nature of the CPS line allows to place the diode and load resistor $R_L = 2.5\,\text{k}\Omega$ in a shunt topology between the CPS branches.

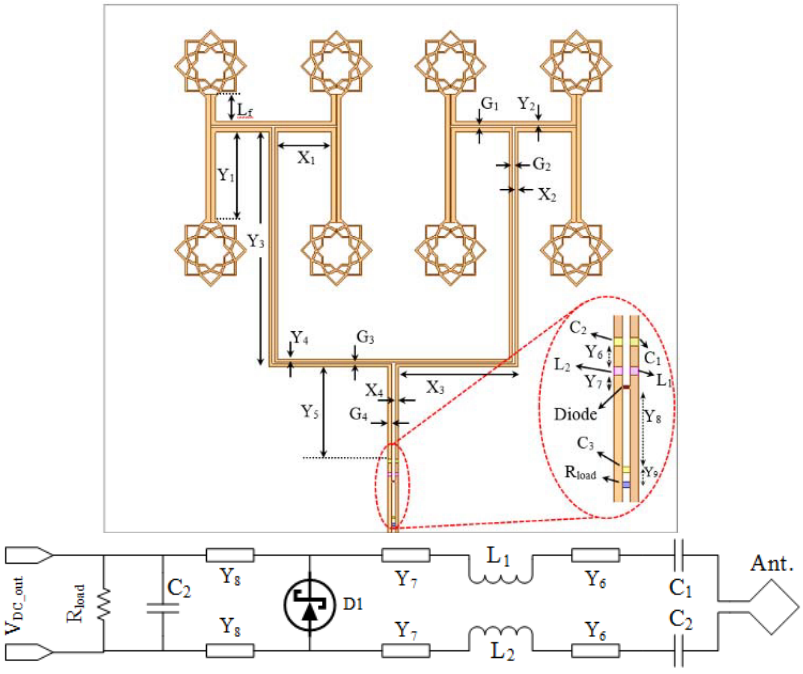

Figure 17. Designed fractal CPS-fed array rectenna.

The values for the employed components and length of the lines between them have been determined from simulated and measured data for impedance matching while achieving an acceptable RF-to-DC power conversion efficiency (PEC) at low input powers. The DC-pass $C_3 = 330\,\text{pF}$ acts as a shorted stub matching network and tunes out the diode reactance. It smoothens the DC output voltage and also allows the remixing of the power at the harmonic frequencies. The optimal distance between the diode and DC-pass filter and the distance between the load and DC-pass filter were determined to be $Y_8 = 23.2\,\text{mm}$ and $Y_9 = 3\,\text{mm}$, respectively. The $C_1 = C_2 = 0.2\,\text{pF}$ capacitors, $L_1 = L_2 = 16.1\,\text{nH}$ inductors, and the length of the CPS line $Y_6 = 6.18\,\text{mm}$ between them and the length of the CPS line $Y_7 = 3\,\text{mm}$ are used to conjugate match the array antenna impedance to the diode impedance at 2.4 GHz. The matching circuit also acts as a filter that prevents the leakage of the higher-order harmonics, generated by the diode, to the antenna and sends them back to the diode to get remixed and generate more DC power. The C_1 and C_2 capacitors also provide the DC isolation between the array antenna and the rectifier.

A prototype of the proposed array rectenna was realized by integrating the designed rectifier and array antenna, and measurements were performed to investigate its performance. The fabricated rectenna array is shown in Fig. 18, and the measurement setup is shown in Fig. 19, where a standard horn antenna with a gain level of 9 dBi is placed at a distance of 2 m to feed the array rectenna while satisfying the far-field criteria. A Ceyear-1441B RF signal generator is connected to the horn antenna through an Analog Devices ADL5321 amplifier to provide adequate controllable and detectable power to the rectenna array.

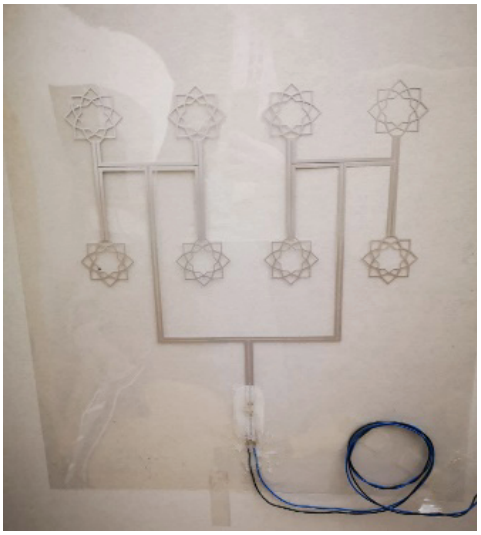

Figure 18. Fabricated array rectenna.

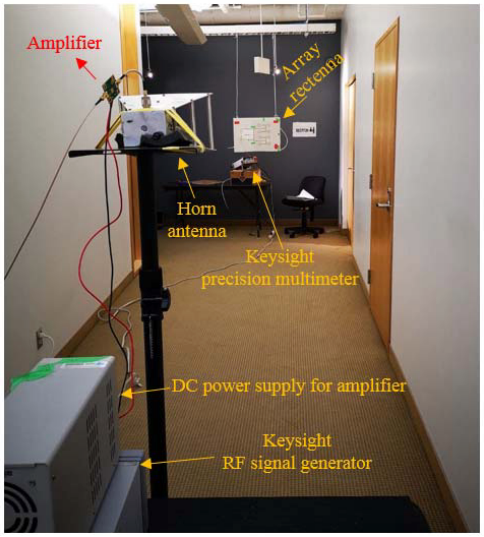

Figure 19. Measurement setup for the proposed array rectenna.

The employed amplifier is capable of providing a maximum gain of 14 dB at 2.4 GHz. An Agilent-34401A precision multimeter is connected in parallel with the load resistance of the array rectenna to measure the output DC voltage. Before performing the measurements on the array rectenna, a dipole antenna with a known gain of 2 dBi was placed at the same location of the array rectenna, and the received power was measured by an Anritsu MS2724B spectrum analyzer. Then the corresponding available power density in space was calculated accordingly.

The measured and simulated results for the RF-to-DC PCE and the output voltage are compared in Fig. 20. The ground-plane less structure of the rectenna allows it to capture the RF energy from its back and front. The measurements were performed for both cases. The measured results reveal that for the case in which the array rectenna was illuminated from its front, it provides a PCE $> 20\%$ for the incident power densities greater than 0.025 $\mu\text{W/cm}^2$ with a peak PCE of 61.3% at $4.03\,\mu\text{W/cm}^2$.

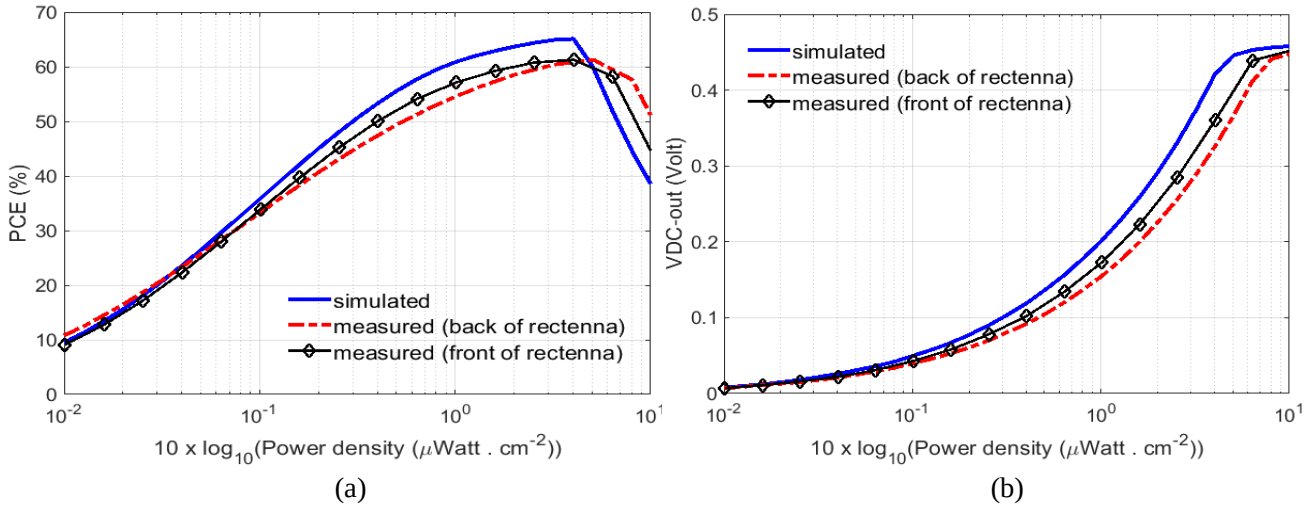

Figure 20. Measured and simulated results: (a) RF-to-DC PCE for various values of the load resistance, and (b) output DC voltage for various values of the load resistance.

Table 4. Comparative analysis of proposed rectenna with other existing rectennas.

Reference	Frequency (GHz)	Rectenna Type	Substrate	Gain (dBi)	Transmission distance (m)	Max. Conversion efficiency
[8]	2.42	single	FR-4	3.93	2	78.53% at 0 dBm
[9]	1.975–4.744	single	FR-4	4.3	2	88.58% at 0 dBm
[10]	2.45	array	FR-4	Not reported	0.5	65.3% at 5 dBm
[11]	9.5	array	Rogers RO4003	11.2	0.25	71.9% at 50.1 mW
This work	2.4 GHz	array	gypsum	9.96	2	61.3% at 4.03 μW/cm^2 power density

The corresponding DC output voltages are 0.022 V and 0.44 V, respectively. For the case in which the array rectenna was illuminated from its back, it provides PCE $>$ 20% for the incident power densities greater than 0.028 μW/cm^2 with a peak PCE of 61.3% at 5.07 μW/cm^2. The corresponding DC output voltages are 0.022 V and 0.44 V, respectively. Very fine agreement exists between the measured results and simulation predictions. The slight deviation is mainly due to the fabrication and setup precision.

Table 4 provides a comparison between the results achieved in this work against the existing works in the literature. The proposed rectifier provides a suitable conversion efficiency at very low input powers delivered to it and for a resistive load of 2.5 kΩ. This verifies its capability to work with different low-power devices for IoE applications.

4. CONCLUSION

In this paper, the design of a flat-bed screen printed CPS-fed fractal folded antenna element/array and rectenna has been presented and discussed. The performance of the radiating antenna elements printed on a thin PET substrate and implemented on various common building materials such as gypsum, plexiglass, and plywood were investigated and experimentally verified. Simulation and measurement results reveal that these materials can be used effectively as the substrate for massive deployment of the IoE technology. Moreover, using the already existing building materials as the substrate not only reduces the implementation costs but also provides an environmentally friendly approach. Besides, the amount of the utilized silver ink for the printing process is significantly reduced due to the groundless structure of the presented CPS-fed element/array.

The designed eight-elements fractal array provides 9.96 dBi gain characteristic at 2.4 GHz ISM-band which is suitable for WPT applications under low ambient energy circumstances. The experimental results show that the proposed array rectenna is capable of providing more than 20% PCE for incident power densities as low as 0.028 $\mu W/cm^2$ while having a peak PCE of 61.3% occurring for a low incident power density of 5.07 $\mu W/cm^2$, which is corresponding to delivering a DC voltage of 0.44 V to a 2.5 kΩ load. The achieved results reveal that the presented array rectenna and the proposed methodology could be a suitable candidate for massive deployment of the wireless sensors network for IoE technology. In the future, the printing process can be used directly on the dry-wall material to reduce the cost with a performance-enhancing.

REFERENCES

1. Rajus, V. S., J. Boi-Ukeme, R. S. Jiresal, et al., "Measured data reliability for building performance and maintenance," *IEEE Instrumentation & Measurement Magazine*, Vol. 25, No. 1, 55–61, Feb. 2022.
2. Mahmoud, A., H. Sadruddin, P. Coser, and M. Atia, "Integration of wearable sensors measurements for indoor pedestrian tracking," *IEEE Instrumentation & Measurement Magazine*, Vol. 25, No. 1, 46–54, Feb. 2022.
3. Chen, S., J. Wang, L. Zhang, et al., "When internet of things meets e-health: An indoor temperature monitoring and control approach," *IEEE Internet of Things Magazine*, Vol. 4, No. 3, 12–16, Sep. 2021.
4. Sotres, P., J. R. Santana, L. Sánchez, J. Lanza, and L. Muñoz, "Practical lessons from the deployment and management of a smart city internet-of-things infrastructure: The SmartSantander testbed case," *IEEE Access*, Vol. 5, 14309–14322, 2017.
5. Yu, B.-Y., Z.-H. Wang, L. Ju, et al., "Flexible and wearable hybrid RF and solar energy harvesting system," *IEEE Transactions on Antennas and Propagation*, Vol. 70, No. 3, 2223–2233, Mar. 2022.
6. Tan, T., Z. Yan, H. Zou, K. Ma, F. Liu, L. Zhao, Z. Peng, and W. Zhang, "Renewable energy harvesting and absorbing via multi-scale metamaterial systems for Internet of things," *Applied Energy*, Vol. 254, 2019.
7. Ferreira, D., L. Sismeiro, A. Ferreira, R. F. S. Caldeirinha, T. R. Fernandes, and I. Cuiñas, "Hybrid FSS and rectenna design for wireless power harvesting," *IEEE Transactions on Antennas and Propagation*, Vol. 64, No. 5, 2038–2042, May 2016.
8. Pandey, R., A. K. Shankhwar, and A. Singh, "Design and analysis of rectenna at 2.42 GHz for Wi-Fi energy harvesting," *Progress In Electromagnetics Research C*, Vol. 117, 89–98, 2021.
9. Pandey, R., A. K. Shankhwar, and A. Singh, "An improved conversion efficiency of 1.975 to 4.744 GHz rectenna for wireless sensor applications," *Progress In Electromagnetics Research C*, Vol. 109, 217–225, 2021.
10. Chuma, E. L., Y. Iano, M. S. Costa, L. T. Manera, and L. L. B. Roger, "A compact-integrated recon gurable rectenna array for RF power harvesting with a practical physical structure," *Progress In Electromagnetics Research M*, Vol. 70, 89–98, 2018.
11. Shin, J., M. Seo, J. Choi, J. So, and C. Cheon, "A compact and wideband circularly polarized rectenna with high efficiency at X-band," *Progress In Electromagnetics Research*, Vol. 145, 163–173, 2014.
12. Zhekov, S. S., O. Franek, and G. F. Pedersen, "Dielectric properties of common building materials for ultrawideband propagation studies [measurements corner]," *IEEE Antennas and Propagation Magazine*, Vol. 62, No. 1, 72–81, Feb. 2020.
13. Baker-Jarvis, J., M. Janezic, B. Riddle, R. Johnk, C. Holloway, R. Geyer, and C. Grosvenor, "Measuring the permittivity and permeability of lossy materials: Solids, liquids, metals, and negative-index materials," Technical Note (NIST TN), National Institute of Standards and Technology, Gaithersburg, MD, 2005.
14. Cuiñas, I. and M. G. Sánchez, "Permittivity and Conductivity Measurements of Building Materials at 5.8 GHz and 41.5 GHz," *Wireless Personal Communications*, Vol. 20, 93–100, 2002.

15. Cuiñas, I., et al., "Frequency dependence of dielectric constant of construction materials in microwave and millimeter-wave bands," *Microwave and Optical Technology Letters*, Vol. 30, 123–124, 2001.
16. Antoine, R., "Dielectric permittivity of concrete between 50 MHz and 1 GHz and GPR measurements for building materials evaluation," *Journal of Applied Geophysics*, Vol. 40, 89–94, 1998.
17. Oliveira, J. G. D., J, G. D. Junior, . N. M. G. Pinto, et al., "A new planar microwave sensor for building materials complex permittivity characterization," *Sensors*, Vol. 20, No. 21, 6328, 2020.
18. Nepa, P. and H. Rogier, "Wearable antennas for off-body radio links at VHF and UHF bands: Challenges, the state of the art, and future trends below 1 GHz," *IEEE Antennas and Propagation Magazine*, Vol. 57, No. 5, 30–52, Oct. 2015.
19. Del-Rio-Ruiz, R., J. Lopez-Garde, J. Legarda, S. Lemey, O. Caytan, and H. Rogier, "Reliable lab-scale construction process for electromagnetically coupled textile microstrip patch antennas for the 2.45 GHz ISM band," *IEEE Antennas and Wireless Propagation Letters*, Vol. 19, No. 1, 153–157, Jan. 2020.
20. Sipilä, E., J. Virkki, L. Sydänheimo, and L. Ukkonen, "Experimental study on brush-painted metallic nanoparticle UHF RFID tags on wood substrates," *IEEE Antennas and Wireless Propagation Letters*, Vol. 14, 301–304, 2015.
21. Verma, A., C. Fumeaux, V. T. Truong, and B. D. Bates, "A 2 GHz Polypyrrole microstrip patch antenna on Plexiglas substrate," *2009 Asia Pacific Microwave Conference*, 36–39, 2009.
22. Youn, S., D. Jang, N. K. Kong, and H. Choo, "Design of a printed 5G monopole antenna with periodic patch director on the laminated window glass," *IEEE Antennas and Wireless Propagation Letters*, Vol. 21, No. 2, 297–301, 2022.
23. Multi-Plastics, http://multi-plastics.com/ (accessed Oct. 16, 2022).
24. Novacentrix, "Metalon conductive inks for flexible printed electronics," https://www.novacentrix.com/ (accessed Oct. 16, 2022).
25. Vandelle, E., D. H. N. Bui, T. Vuong, G. Ardila, K. Wu, and S. Hemour, "Harvesting ambient RF energy efficiently with optimal angular coverage," *IEEE Transactions on Antennas and Propagation*, Vol. 67, No. 3, 1862–1873, Mar. 2019.
26. Bruker, "High-value life science and material research and diagnostics solutions," https://www.bruker.com/en.html (accessed Oct. 16, 2022).
27. Testing Machines Inc., Industrial Physics, "Materials testing," https://industrialphysics.com/brands/testing-machines-inc/ (accessed Oct. 16, 2022).
28. Signatone, https://signatone.com/ (accessed Oct. 16, 2022).
29. Chen, E. and S. Y. Chou, "Characteristics of coplanar transmission lines on multilayer substrates: Modeling and experiments," *IEEE Transactions on Microwave Theory and Techniques*, Vol. 45, No. 6, 939–945, Jun. 1997.
30. Goverdhanam, K., R. N. Simons, and L. P. B. Katehi, "Coplanar stripline components for high-frequency applications," *IEEE Transactions on Microwave Theory and Techniques*, Vol. 45, No. 10, 1725–1729, Oct. 1997.
31. Antonio Estrada, J., E. Kwiatkowski, A. López-Yela, et al., "RF-harvesting tightly coupled rectenna array tee-shirt with greater than octave bandwidth," *IEEE Transactions on Microwave Theory and Techniques*, Vol. 68, No. 9, 3908–3919, Sept. 2020.